Wind Stress from Wave Slopes Using Phillips Equilibrium Theory

BARBARA-ANN JUSZKO

Juszko Scientific Services, Victoria, British Columbia, Canada

RICHARD F. MARSDEN AND SHERMAN R. WADDELL

Physics Department, Royal Roads Military College, FMO, Victoria, British Columbia, Canada

(Manuscript received 25 January 1993, in final form 15 February 1994)

ABSTRACT

An open ocean, deep water air–sea interaction experiment was conducted in the Gulf of Alaska. Wave amplitude and slope data were measured using a WAVEC heave, pitch, and roll buoy that was let drift in the Alaska gyre. Wind stress estimates were obtained from a fast-sample anemometer using the dissipation technique and from synoptic measurements through a boundary-layer model. The fundamental correlation and predictive relationships between wind friction velocity and wave spectral properties were established. A comparison of the slope spectrum to simultaneous wind stresses allowed us to estimate the Phillips proposed universal constant β. Reintroducing this constant β into the Phillips slope spectrum and using measured slope spectral characteristics, an inferred wind stress was calculated that was shown to agree well with both the dissipation and model stresses thereby validating both Phillips theory and the boundary-layer model. Any discrepancies with the model stresses were attributed to second-order wave age effects. The roughness length z_0, nondimensionalized by the sea rms wave height, was shown to decrease with wave age in a manner consistent with Kitaigorodskii's functional form. A general expression for C_d as a function of wind speed or friction velocity and wave age was proposed and verified with independent data.

1. Introduction

The close relation between the variance of the surface slope spectrum and wind speed has long been recognized. The classic result is that of Cox and Munk (1954) in which they infer total wave slope statistics from photographs of sea surface glitter observed by aircraft-mounted cameras and compare the results to simultaneous ship wind speed measurements. Marsden and Juszko (1989), using a WAVEC heave, pitch, and roll buoy, were able to show a close relationship between the variance of a much more limited portion of the wave slope spectrum and the speed and direction of an inferred surface wind. A major weakness of the latter study was that the anemometer was located at the top of a drill rig, 80 m above the water surface. Smith's (1988) boundary-layer model was used to correct the winds to 10-m height and conditions of neutral stability. The correction to the sea surface relies critically on the existence of the "constant stress layer," which could not be justified under all stability conditions. A simple regression between the variates revealed, however, an extremely high correlation coefficient (0.90 in wind speed) and a model rms error that was equivalent to, or smaller than, other wind inference techniques.

Of much wider interest, however, is the wind stress τ, because it represents the momentum transfer from the atmosphere to the ocean. Consequently, the theory of air–sea interaction, for the most part, is cast in terms of the friction velocity $u_* = (\tau/\rho)^{1/2}$, where ρ is the density of air. Operationally, the wind stress is inferred through the bulk aerodynamic flux formula:

$$\tau = \rho C_d(u)|u|\mathbf{u},$$

where $C_d(u)$ is the drag coefficient, which relates the turbulent Reynolds stresses to the mean wind vector $\mathbf{u}$. Several authors, (e.g., Smith et al. 1992; Marsden et al. 1993) have suggested that a second-order correction to this relation may be required to account for wave age. This is a recognition that the roughness elements (i.e., waves or wave slopes), which drive the turbulent eddy fluctuations inherent in the wind stress, may take a finite amount of time to develop, producing an apparent disequilibrium between the mean wind and the actual wind stress under changing wind conditions.

Phillips (1985) has presented a complete theory of the response of the sea surface to wind stress in which he proposes a direct relation between the sea surface slope spectrum and the wind stress in the equilibrium range. The rate of change of spectral action density (N)

Corresponding author address: Ms. Barbara-Ann Juszko, Juszko Scientific Services, 127 Cliff Dr. RR #4, Victoria, BC V9B 5T8 Canada.

for wind-generated surface gravity waves in space and time can be expressed as

$$\frac{\partial N(\omega, \theta)}{\partial t} + C_g \cdot \nabla N(\omega, \theta) = S_{NL} + S_W + S_{DIS}, \quad (1)$$

where $C_g \cdot \nabla N$ represents advection by the wave group velocity C_g, S_{NL} is the change in action density due to nonlinear wave–wave interaction, S_W is the input by the wind, and S_{DIS} is the loss due to wave breaking. In fetch unlimited conditions, the advective term is assumed negligible. In the equilibrium range of the spectrum, the timescale of growth becomes large compared to the internal redistribution timescale, and a state of statistical equilibrium exists such that

$$S_{NL} + S_W + S_{DIS} = 0. \quad (2)$$

Phillips (1985), assuming this statistical balance and that the three terms are of equal importance, established a theoretical expression for the wavenumber spectra from which the frequency spectra and, of particular interest in this paper, the spectra of sea surface slope were derived. According to Phillips [his Eq. (3.16)], the total sea surface slope frequency spectrum in the equilibrium range is

$$S(\omega) = 4\beta I(p) u_* g^{-1}, \quad (3)$$

where u_* is the wind friction velocity, β is a proposed universal constant, g is the gravitational acceleration, and $I(p)$ is

$$I(p) = \int_{-\pi/2}^{\pi/2} \cos^p \theta d\theta. \quad (4)$$

This expression indicates that the spectrum of total slope is flat in the equilibrium range (i.e., no frequency dependence), varies directly with u_*, is independent of the sea spectral peak frequency and, most importantly, requires only one parameter, β, for its description.

If one can validate Eq. (3) and demonstrate that β is in fact a constant, then deductions can be made on the relationships between wind stress and sea state, which can be examined theoretically or used in prediction. Furthermore, an inferred wind stress from sea state properties should include all first- and second-order corrections that normally are applied to anemometer wind speed/stress estimates. Assuming a constant stress layer (i.e., a region exists where u_* is invariant with height above the sea surface) and that all properties are adjusted for corrections due to air column stability, the velocity profile is given by the familiar "law of the wall":

$$u(z) = \frac{u_*}{\kappa} \ln\left(\frac{z}{z_0}\right), \quad (5)$$

where $\kappa = 0.4$ is von Kármán's constant, $u(z)$ is the wind speed at height z, and z_0 is the virtual origin of the profile representing a "roughness length." The first-order correction takes into account the stability of the air column, while a second-order correction is needed due to interaction between the roughness elements of the sea surface (i.e., sea state), contained in z_0, and the velocity profile. That is, although the sea state is in equilibrium with u_*, it may be in disequilibrium with $u(z)$. This disequilibrium is identified by the variability of the roughness length z_0 with wave age expressed as either C_p/u_* or C_p/u_{10}, where C_p is the phase speed of the dominant sea waves.

From an experimental point of view, one can measure the slope spectrum directly from the tilt sensors of a directional buoy or calculate an equivalent slope spectrum from the amplitude spectrum

$$E(\omega) = 4\beta I(p) u_* g \omega^{-4} \quad (6)$$

by multiplying both sides of the equation with ω^4. In either case, it is easier to search for a flat region in the slope spectrum and find a mean $S(\omega)$ value than to fit a line to an ω^{-4} high frequency tail. Any deviation from a zero slope frequency relation can be readily identified. Furthermore, if $S(\omega)$ is invariant with frequency, one needs only a portion of the equilibrium range to perform the mean calculation. However, it should be noted that sea surface slope estimates are mechanically easier to obtain in the open ocean by directly measuring tilt using pendulum sensors or flux-gate magnetometers than amplitude values, which generally require the double integration of a vertical acceleration.

In February 1992, a multiship experiment was conducted in the Gulf of Alaska as part of the Critical Sea Test 7 (CST-7) program. The primary purpose of the study was to link air–sea boundary processes with scattering theory related to surface acoustic measurements. Experiments were conducted to measure subsurface bubble clouds, breaking surface waves, water column structure, and sonar reflection. Complementary environmental information was gathered including wind speed and direction measurements, dissipation wind stress estimates, and directional wave spectra. The experiment was unique because it was conducted in open ocean, fetch unlimited conditions, and in very deep water (greater than 5000 m). The wave data were obtained from a drogued surface-following buoy. In this paper, we will use the environmental information to establish the fundamental correlation and prediction structure between wave parameters and wind stress to verify the Phillips proposed spectral shape, to validate Smith's (1988) boundary-layer model, and to obtain an estimate for β. The constant nature of β will be demonstrated, and we will show that the wave-inferred friction velocities (u_*) are consistent with the dissipation observations. Using accepted air–sea interaction relationships and our observed wind stress/wave height prediction, a simple theoretical development will lead to the establishment of a general equation describing

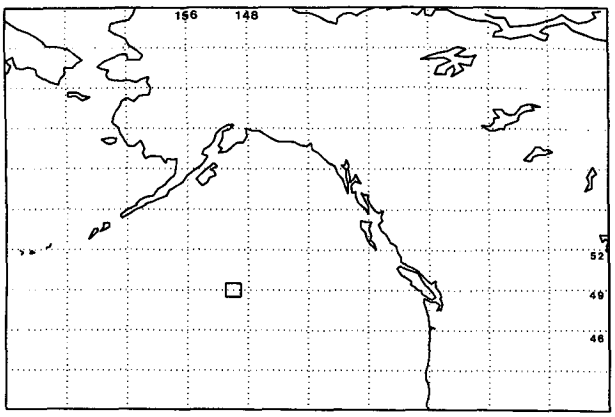

FIG. 1. Study location.

the relationship between the drag coefficient, wind speed, and wave age.

The paper will be organized in the following manner. Section 2 will describe the experimental design and data analysis procedures. Section 3 will discuss the wind and wave observations and describe the correlation relationships between spectral properties and measured u_* (3a). Then β will be calculated and its behavior assessed leading to an estimate of slope-inferred u_* (3b). In section 4, the wind stress–sea state relationships will be determined through examination of the behavior of z_0 in light of historical findings and the results of section 3. The paper will conclude with a summary and discussion in section 5.

2. Data collection

The experiment extended from 24 February through 29 February 1992 (Julian day 55 through 60) in the region shown in Fig. 1. It involved the participation of two research vessels, the CSS *J.P. Tully* and the *Cory Chouest*. Each ship was equipped with an R. M. Young anemometer, which supplied wind speeds and directions measured at a nominal height of 19.5 m above the surface and sampled every 15 min on the *Cory Chouest* and 30 min on the *Tully*. Concurrent air–sea temperature and humidity differences were input into Smith's (1988) boundary-layer model to produce model estimates of wind stress and 10-m wind speed. These stresses are corrected for stability but not for second-order wave age effects. A fast-sampling R. M. Young anemometer (model RE05701) was mounted on the masthead of the Tully, within 2 m of the slower response anemometer, in order to obtain dissipation wind stress estimates and to verify the model stresses. A Datawell WAVEC slope-following buoy was drogued to 100 m and left to float freely in the experimental area to transmit vertical displacement and slope measurements to the *Tully*. The drogue allowed the wave buoy to travel with the surface currents eliminating concerns about Doppler shift due to the mean current and provided sufficient downward tension to prevent overturning and inaccurate surface following. Primary position was telemetered through an ARGOS satellite transmitter with an HF radio transmitter used as backup. Continuous surface displacement and vector slopes were telemetered every 0.78125 seconds from the buoy to a DIREC receiver and then stored on a microcomputer using standard computer software. Spectra were postcalculated every 30 minutes, on blocks of 128 points, providing 18 blocks for the ensemble averaging and 64 co- and quadspectral estimates with a frequency resolution of 0.01 Hz. Directional spectra were then obtained using the noniterative eigenvector method of Marsden and Juszko (1987).

Because the accurate response of the buoy to sea surface slopes is critical to the analysis in this paper, a short discussion of its response verification is justified. It has been suggested that due to its size, 2-m diameter, the WAVEC buoy does not respond linearly to the wave slope field in its frequency measurement band (0.01–0.64 Hz). It can be readily shown that a buoy estimate of the scalar wavenumber can be found from

$$k_{\text{buoy}} = \left(\frac{C_{O_{11}} + C_{O_{22}}}{C_{O_{00}}} \right)^{1/2}, \tag{7}$$

where $C_{O_{11}}$ and $C_{O_{22}}$ are the power spectral densities of the east–west and north–south slopes, respectively, and $C_{O_{00}}$ is the power spectral density of the wave amplitude. Assuming a deep water dispersion relation ($k_{\text{theoretical}} = \omega^2/g$), one can independently verify whether the buoy calibrations have been correctly applied. Figure 2 shows the ratio of $k_{\text{theoretical}}/k_{\text{buoy}}$ as a function of frequency for a typical 30-min period. From 0.01 to 0.05 Hz, the theoretical response is not followed, while from 0.05 to 0.50 Hz the agreement is very good. Above 0.5 Hz, the ratio again departs from the expected value of 1.0. Since the sea portion of the spectrum did

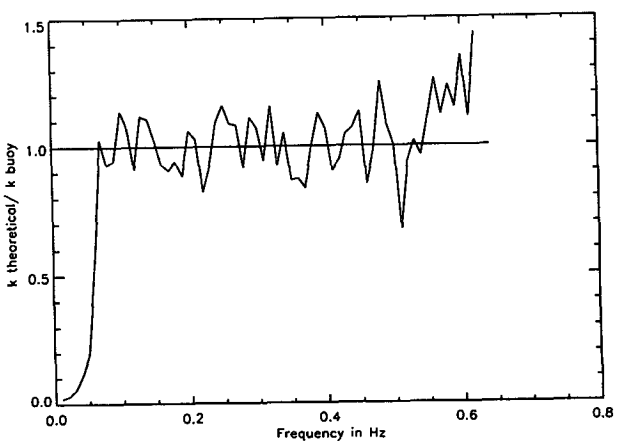

FIG. 2. Buoy response as a function of frequency. (See Eq. 7.)

not develop below 0.05 Hz, we are not concerned with errors in this frequency band. The high frequency errors may be due to 1) nonlinear response in the wave amplitude leading to an overestimate of its spectral density, 2) nonlinear response in the wave slope resulting in its underestimate, or 3) Doppler shifting caused by short waves riding on the velocity field of the long waves. We will show in section 3a the development of the slope and amplitude spectra during a rising wind and that the slope spectra maintain their shape to the Nyquist frequency. Consequently, we suggest that the high frequency ratio mismatch is due to errors in the amplitude response derived from a double integration of the vertical acceleration rather than due to the buoy-measured wave slopes. This will be verified through examination of the wave statistics in section 3a. Our analysis, therefore, will utilize the direct slope estimates as opposed to an equivalent slope obtained through multiplication of the amplitude spectrum by ω^4. To protect against the possibility of Doppler shift errors, as will be discussed presently, the averaging range was truncated for high wind conditions.

The fast-sampling R. M. Young anemometer was located on the *Tully* and had an effective response length of 0.8 m. Instead of the usual recording of the number of revolutions per unit time, we recorded the time interval and wind direction corresponding to 1.0 m of wind run in order to fully exploit the resolution of the instrument at both low and high wind speeds while minimizing data storage requirements. The wind components were then spline fit to equal 60 s/1024 = 0.0589 s intervals corresponding to a 17.1-Hz sampling rate. The friction velocity u_* was then determined by the inertial dissipation method ($u_{*\text{diss}}$) according to Marsden et al. (1993). The spectra for 1-minute groups (eight sets of 128 points) were calculated and the inertial subrange was determined visually for each. This was critical to the calculation as the wave field was swell dominated and ship motion was evident in the wind record. If an inertial subrange could not be discerned, the 1-min run was rejected. The environmental information was then used to correct the data for stability. Unfortunately, we experienced recording problems and obtained only a limited number of fast-sampling wind records. There were enough, however, to verify and add support to inferences made based on the Smith (1988) boundary-layer model. Furthermore, the study will present stresses calculated from the *Tully* and model results from the *Cory Chouest,* thus ensuring data independence. Both the 15-min, 10-m synoptic model winds and the one-minute dissipation wind stresses were averaged over the corresponding 30-minute wave sample interval. In the case of the discontinuous wind stress time series, 30 one-minute samples were not always available, so that each estimate may reflect varying experimental noise levels. As the input datasets came from differing locations in the experimental area (i.e., winds from the *Cory Chouest,* wind stress from the *Tully,* and a drogued WAVEC buoy), one may expect that site differences could influence the analysis. However, Marsden (1987) showed that the correlation length scales in the North Pacific geostrophic winds are very large, on the order of 1200 km, and the reader will see in section 3 that site separation cannot be discerned in the data as the differences are hidden in the noise level of the stresses.

The analysis in this paper requires separation of the wave spectrum into swell, sea, and equilibrium range components. Swell and sea were delimited by the frequency f_{cut}, where the equivalent deep water surface gravity wave phase speed was equal to the observed 10-m neutral wind speed (i.e., $u_{10}/C = 1.0$). Here we make the standard assumption that the wind can force only waves that travel with a slower phase speed. The overall spectral peak frequency f_p was taken as the frequency associated with the maximum $E(f)$ value of the surface displacement spectrum. The location of the sea spectral peak f_{sea} was found at the frequency associated with the maximum $D(f, \theta)$ value of the directional spectrum, along the observed wind direction and with an associated phase speed less than or equal to the wind speed. To avoid the unstable region near the spectral peak and possible Doppler shift effects at higher frequencies due to long sea waves from entering the calculations, the lower and upper bounds for the equilibrium range were then taken as

$$f_1 = 1.5 f_{\text{sea}} \quad (<0.64 \text{ Hz})$$
$$f_2 = 3.0 f_{\text{sea}} \quad (\leq 0.64 \text{ Hz}). \tag{8}$$

The choice of the upper limit is further supported by the results of Banner (1991), who examined the effect of Doppler shifting on the high frequency spectral tail with data from the LEWEX experiment. The lower bound limits the analysis to winds greater than approximately 3.7 m s^{-1} (i.e., the phase speed associated with the maximum acceptable sea peak frequency of 0.42 Hz or $f_1 = 0.63$ Hz). Doppler shift effects due to swell were not considered a serious problem as their direction of travel was generally different from that of the wind-forced waves.

As wind stress is closely linked to the existing sea state, many air–sea properties are examined as a function of wave age given by C_p/u_* or C_p/u_{10}. We will be using the wind stress relation (C_p/u_*) throughout the paper for two reasons. First, our ship winds were initially measured at 19.5-m height and a correction to a 10-m reference height was required that uses the constant stress layer relationship of Eq. (5). If a strong wave age dependence on z_0 exists, which is not included in the model, then an error is being introduced into u_{10} that can contaminate the results. Second, and more importantly, it is the friction velocity that is involved in performing "work" on the sea surface and not the wind speed.

3. Results

a. Observed wind and wave climate

Figure 3 contains the time series of the 10-m neutral wind speed, direction, and wind friction velocity obtained from the synoptic-scale anemometer on the *Cory Chouest* and from the fast-sampling anemometer on the *Tully*. With a maximum wind speed of 16 m s^{-1}, the wind conditions were low to moderate and the discussion will focus on the six events noted on Fig. 3. Figure 3a shows two wave growth periods in events 1 and 2. The increase in wind speed for event 1 is accompanied by considerable wind veering, whereas the directions remained steady during event 2. (See Fig. 3b.) A third wind buildup is seen as event 3 followed by a short lull (less than 6 h) noted as event 4 with a resumption of moderate winds in event 5. Wind directions for events 3 and 5 were relatively steady. Event 6 shows a rapid increase of wind speed to approximately 8 m s^{-1}. Both speed and direction then remained relatively constant for approximately 24 h. The time series of $u_{*\text{model}}$ and $u_{*\text{diss}}$ (Fig. 3c) closely follows that of the wind speed. Although the number of dissipation stress records (crosses in the figure) is limited, it can be seen that they correspond well with $u_{*\text{model}}$ over a range of wind speeds including the higher winds of event 5 and, as will be seen presently, reflect a full range of wave ages.

Selected wave parameters are plotted in Figs. 4a–f. Gaps in the time series coincide with periods when the WAVEC buoy had drifted beyond telemetry/receiver range ($\sim$15 n mi). Records in which an equilibrium range could not be found (generally very low wind conditions) were also excluded. Figure 4a shows the time series of the total and sea rms wave height (i.e., the standard deviation of the wave amplitude). Figure 4b illustrates the time series of sea and spectral peak frequency. Both Figs. 4a and 4b indicate that the wave field is swell dominated for most of the study period; therefore, experiments that do not carefully separate the sea component could introduce considerable error into derived statistics. The effect of wave age, which reflects the finite amount of time needed for seas to develop in order to reach maturity under a given wind forcing, can best be observed by examining the wave growth of events 1, 2, 3, and 5. Both u_{10} and u_*, as well as the initial background energy levels, during event 1 are considerably greater than for event 2; however, the spectral growth is slower in event 1 as seen in the progression of sea peak frequency toward lower frequencies. The primary difference between these two events is that the wind direction is veering during event 1 while constant during event 2. Similarly, the sea peak of event 3 (starting at day 56.4 with similar background energy levels) progresses to lower frequencies than event 1 over the same temporal growth period, and the sea peak continues to grow until the wind speed rapidly drops at event 4 (i.e., event 1 is also duration limited). The wave response implies that the u_* felt by the waves should be less than that modeled in event 1, possibly due to wave age considerations. Perhaps the best example of wave age effects is the difference in sea development between event 3 and event 5. The much more rapid response of event 5 may reflect the continued presence of roughness elements that had insufficient time to fully dissipate during the lull of event 4. The sea of event 6 shows rapid sea peak frequency descent from 0.4 to 0.2 Hz after which conditions remained relatively stable with the wave and wind field in equilibrium. Figure 4c shows the equilibrium range frequencies, as defined in Eq. (8), and indicates that the number of frequencies used in the averaging during later analysis will vary. Figure 4d contains the mean wave directions obtained as

$$\bar{\theta} = \text{atan}\left(\frac{\sum Q_{01}(f_j)}{\sum Q_{02}(f_j)}\right), \tag{9}$$

where the sum of quadspectral components (0: heave, 1: east–west, 2: north–south slope) is performed over selected frequency limits (0.03–0.64 for the total spectrum, f_{cut} to 0.64 for the sea, and f_1 to f_2 for the equilibrium range). This figure shows that the total mean wave direction may be contaminated with swell; however, there is usually close agreement between the sea, equilibrium, and wind directions (Fig. 3b).

The shape of the total slope frequency spectrum proposed by Phillips [(1985), Eq. (3)] requires that the equilibrium range be flat. Figures 5a–d, associated with event 6 of Figs. 3 and 4, show the amplitude and total slope frequency spectra for this sea development period (chosen for illustrative purposes). An initial indication of sea development can be seen in Fig. 5a near the Nyquist frequency. Figures 5b–d illustrate a progression of this sea peak toward lower frequencies in both the amplitude and total slope spectra. At frequencies greater than the sea peak (from $\sim 1.5 f_{\text{sea}}$), the slope spectrum is indeed flat up to the Nyquist frequency. The fluctuations in slope spectral density are within two standard deviations of the mean. These observations, therefore, also support a surface displacement spectrum with an ω^{-4} (as opposed to an ω^{-5}) high frequency tail.

To determine β of Eq. (3) requires the calculation of the mean slope spectral density ($\langle S(f) \rangle$) value, averaged over the equilibrium range f_1 to f_2 as defined in Eq. (8), and $I(p)$ defined in Eq. (4). The time series of $\langle S(f) \rangle$ and the standard deviation about this mean are shown in Fig. 4e. It can be seen that the behavior of the mean slope is similar to that of the wind speed and friction velocity (Figs. 3a,c) and rms wave height (Fig. 4a), consistent with the Phillips model. The standard deviation about the mean is relatively constant with slightly higher values during high energy conditions reflecting fewer frequencies used in the averaging.

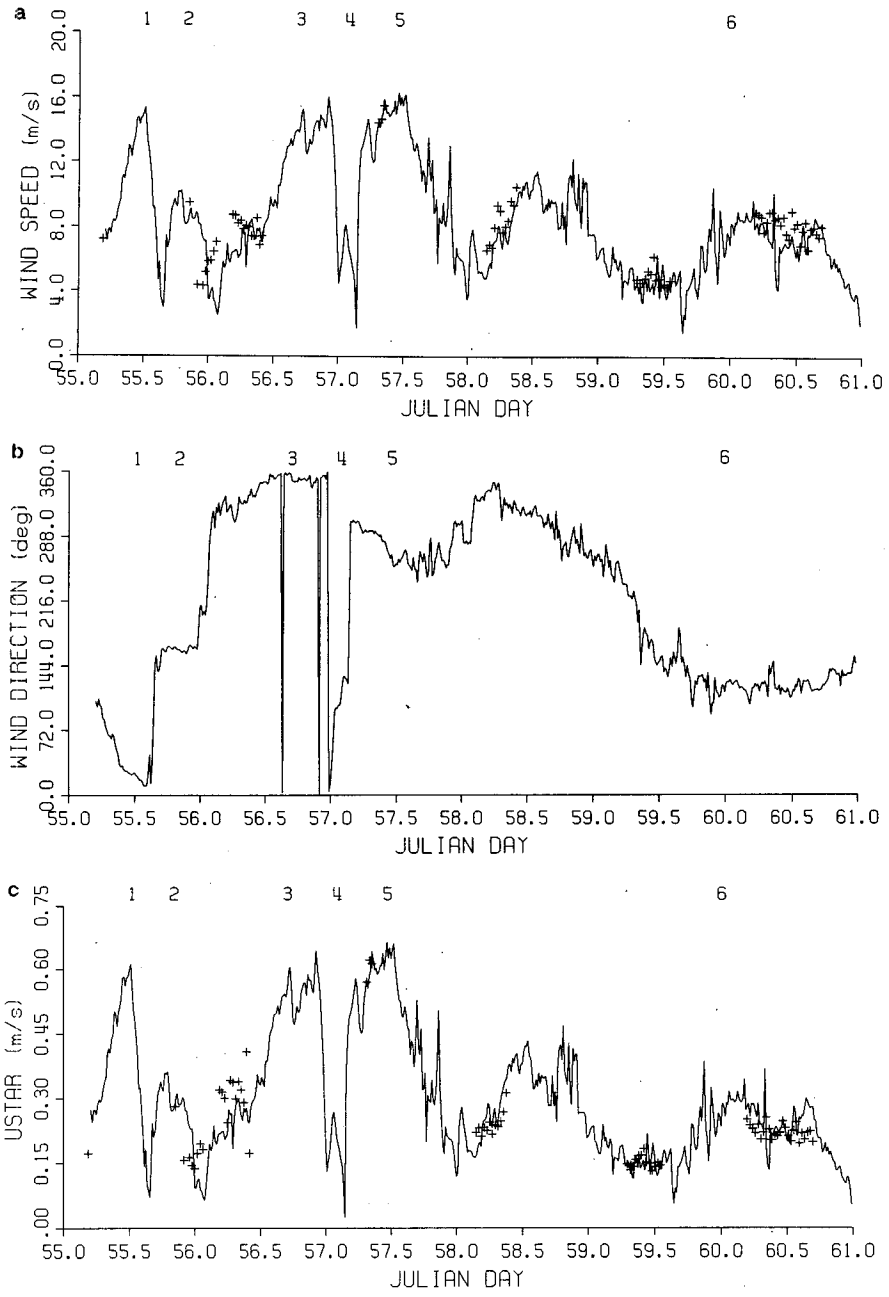

FIG. 3. Time series of (a) wind speed, (b) direction, and (c) friction velocity. Solid line—*Cory Chouest* 10-m winds and $u_{*\text{model}}$; crosses—wind speed and $u_{*\text{diss}}$ from the fast-sampling anemometer on the *Tully*.

According to Phillips [Eqs. (4.10) and (4.11)], the ratio of the total downwind mean-square slope and total rms slope, calculated over the equilibrium range, is equal to $I(p+2)/I(p)$. The slope axes for each 30-min record were rotated to align with the observed *Cory Chouest* wind direction, and the rms slope statistics were calculated over the range f_1–f_2. Some error could be introduced due to the frequency range limits. However, this should be minimal as p does not vary greatly with frequency in the equilibrium range (i.e., if the downwind slope spectral density is constant with f as is the total slope spectral density). The value for p was determined by calculating the ratio of slope values and inverting the known estimates for $I(p+2)/I(p)$, where p ranged from 0.0 to 12.5. The values for this ratio ranged from 0.4 to 0.69, which is slightly broader

than that previously observed by Cox and Munk (1954) of 0.5–0.64. Figure 4f shows the time series of calculated $I(p)$ and indicates a p value normally less than 1.0 and a range from 1.9 to 3.1. There is considerable scatter in the estimate, which severely limited performing quantitative analyses. However, one can note an increase in $I(p)$ (i.e., decrease in p) during the sea development periods of events 1, 3, and 5, implying that p decreases with wave age. Given that many experimental observations show a decrease in the effective wind energy transfer to the sea surface with wave age, a decrease in p, hence a broadening of the directional distribution, implies that the distribution of wind stress roughness elements is being spread away from the mean wind direction, probably due to nonlinear wave–wave interaction, thereby reducing the efficiency of wind energy transfer to the sea surface even though both rms wave height and total wave slope energy increase.

Equation (3) indicates a direct relationship between u_* and $\langle S(f)\rangle$. Figure 6a shows $u_{*\text{model}}$, calculated using Smith's boundary-layer model applied to the *Cory Chouest* winds (dots) and the dissipation friction velocities $u_{*\text{diss}}$ (crosses), obtained from the fast-sampling anemometer on the *Tully* versus $\langle S(f)\rangle$. Clearly a direct relation exists. Similarly, one can examine the relationships between u_* and other wave properties, in particular, C_p and rms sea height. In the case of the latter, a quadratic relationship is expected. The results are shown in Figs. 6b,c. The prediction parameters for a linear model ($u_* = a + bx$), the correlation coefficient, and percent rms error are given in Table 1. The linear regressions for $u_{*\text{diss}}$ are plotted on Fig. 6. The results indicate very high correlations between all three wave spectral properties and wind friction velocity. The best prediction is supplied by the rms sea height, which may be a more stable estimate than either $\langle S(f)\rangle$ or C_p. The C_p regression is weighted toward the lower energy conditions of the $u_{*\text{diss}}$ values. With the exception of u_*^2 versus rms height for the combined dataset when ship model data is included, the y intercept (i.e., value of a) can be considered to be equal to zero. The bulk of the scatter, associated primarily with ship model data, tends to lie above the regression lines. This is consistent with an overestimate of $u_{*\text{model}}$ for a given wave variable when wave age is not taken into account.

Phillips theory provides for the calculation of u_* through the spectral energy density, given in Eq. (6). Since the rms sea height showed the largest correlation with u_*, we have included Fig. 6d, which shows the scatterplot of $\langle f^4E(f)\rangle$ against u_*, with the averaging performed over the same frequency range as $\langle S(f)\rangle$, and the accompanying regression values are listed in Table 1. There are two features to note: 1) fewer records than in the $\langle S(f)\rangle$ analysis could be included due to the occurrence of unrealistically large values of $\langle f^4E(f)\rangle$ and 2) there is a marked increase in the noise level and corresponding reduction in the correlation coefficients, compared to Fig. 6a. On examination of individual records, it became apparent that problems were arising due to contributions to the mean from high frequencies where, as seen in Fig. 2, the buoy amplitude response is no longer linear. Furthermore, the error contribution is dependent on the chosen equilibrium range, hence the sea peak frequency, resulting in an apparent wave age correlation. Therefore, using the amplitude in our equilibrium range analysis would limit it to lower frequency sea peaks (i.e., older waves) and introduce uncertainty due to the possible need for correcting the buoy accelerometer response. This problem is not obvious in the rms sea calculation as energy levels at high frequency are very small compared to the sea peak. If only part of the increased scatter in Fig. 6d is due to instrument response, one may suggest that wave slopes are the more direct link to wind stress than the wave amplitudes.

b. Determination of β and slope inferred u_*

1) CALCULATION OF β

Knowing $\langle S(f)\rangle$, $I(p)$, and u_*, β can now be calculated for each record for both the model and dissipation friction velocities. Estimates of $u_{*\text{model}}$, though corrected for stability, may contain errors due to second-order effects such as wave age (i.e., surface roughness changes). These errors, as well as experimental noise, will propagate through the initial calculation of β from individual wave records and hopefully will cancel on averaging. The resultant time series is shown in Fig. 7. There is considerable noise in these estimates, both from experimental error and possible second-order errors in the $u_{*\text{model}}$ values. To examine the variability in β, the individual estimates were compared to estimates of sea development, (Fig. 8a) (given by the sea spectral peak frequency), directional spread, (Fig. 8b) [using $I(p)$], and direction uncertainty, (Fig. 8c) (given by the difference between mean sea and equilibrium range wave direction as defined in section 3a). These indicate that there appears to be no systematic variation in β with the spectral position of the sea peak or $I(p)$ and that most of the outliers occurred when a direction difference was greater than 20 degrees (reflecting difficulty in properly defining the sea region during some veering events).

2) β AS A FUNCTION OF WAVE AGE

The results of Donelan et al. (1985) and Dobson et al. (1989) suggest that β may be a function of wave age. Consequently, β versus $C_p/u_{*\text{diss}}$ (dissipation estimates only) is plotted in Fig. 8d. The results show an apparent linear relationship between these two variables. Two problems arise with the assumption that β varies with wave age. First, the regression results shown in Table 1 suggest that the three fundamental variates,

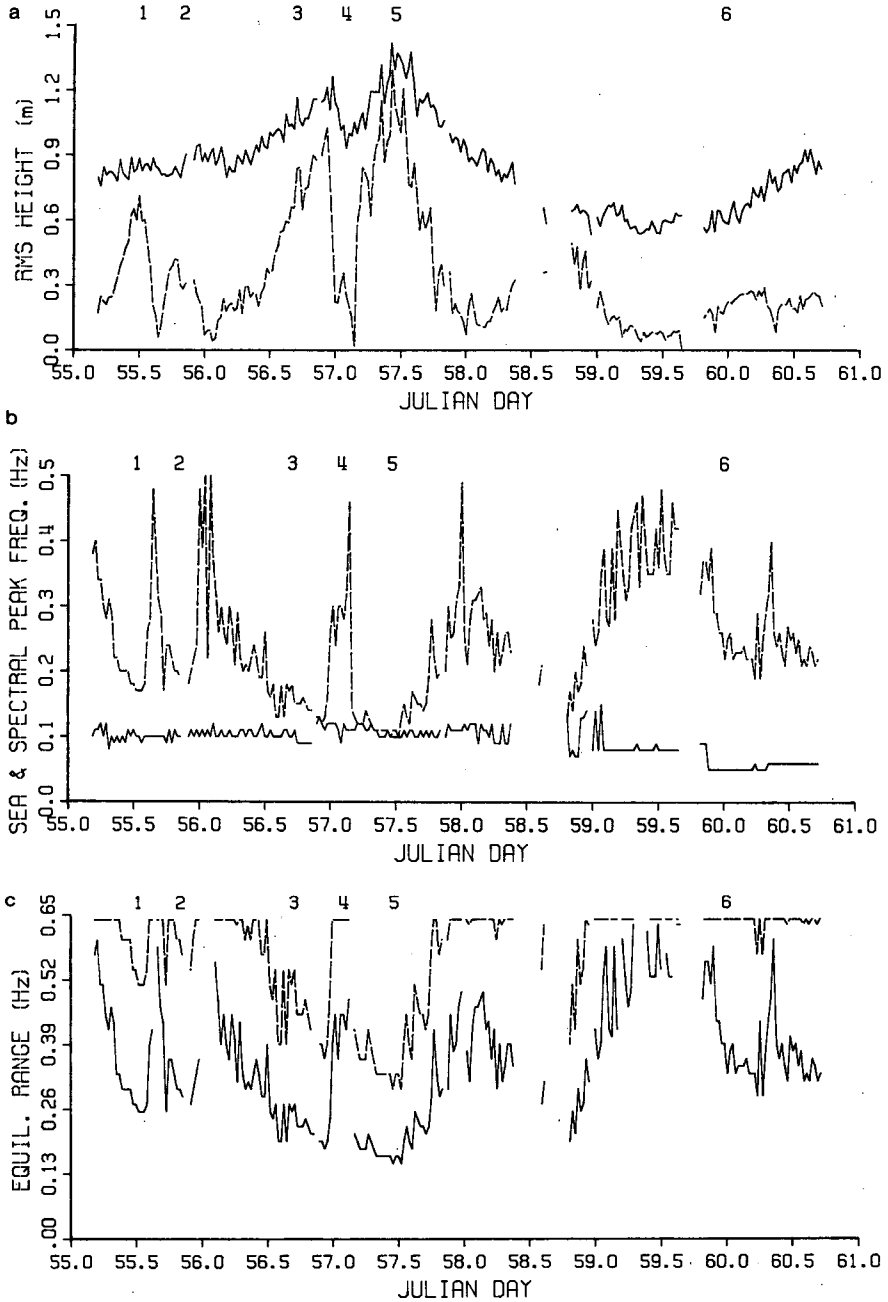

FIG. 4. Time series of wave statistics from the Datawell WAVEC buoy: (a) rms sea (dashed) and total (solid) wave height; (b) sea (dashed) and spectral (solid) peak frequency; (c) lower (solid) and upper (dashed) frequency limits for the equilibrium range; (d) mean wave direction calculated

$\langle S(f)\rangle$, C_p, and $u_{*\mathrm{diss}}$, are all highly correlated. Here β is a transfer function (or constant) relating $\langle S(f)\rangle$ to $u_{*\mathrm{diss}}$. To accept that β is a function of wave age, its inclusion must significantly improve the predictability of $\langle S(f)\rangle$ from $u_{*\mathrm{diss}}$. Consequently, we let β be a linear function of wave age (i.e., $\beta = a + bC_p/u_*$), as suggested by Fig. 8d, and included it in the regression model:

$$\frac{\langle S(f)\rangle g}{I(p)8\pi} = \beta u_* = \left(a + b\frac{C_p}{u_*}\right)u_* = au_* + bC_p.$$

The rms error was 25.6% for a regression model in which β was dependent on wave age and 26.5% for the constant β formulation—a decrease of only 0.9%. The correlation coefficients remained virtually unchanged. Clearly, inclusion of β as a function of wave age pro-

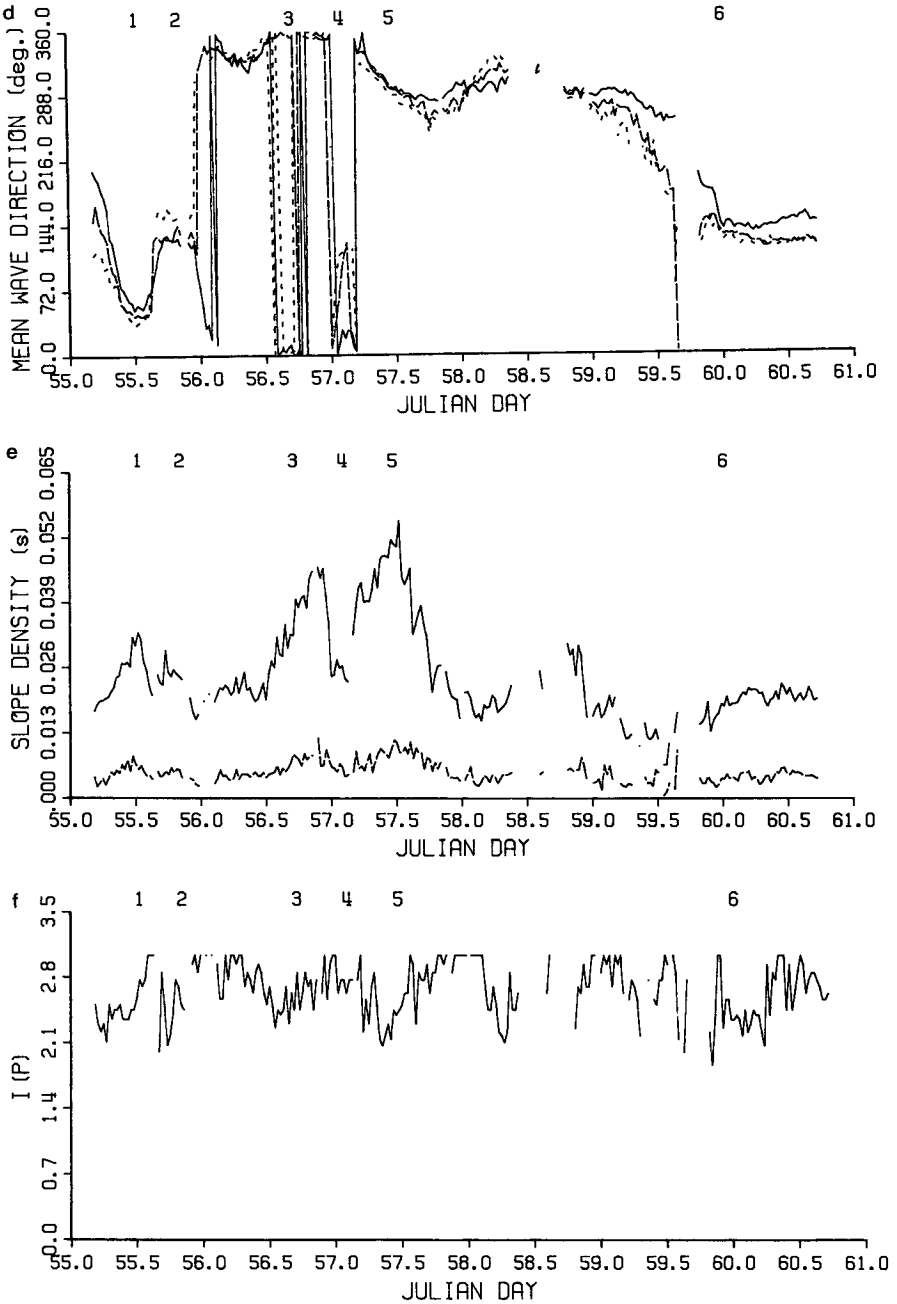

FIG. 4. (*Continued*) over the entire spectrum (solid), the sea portion (long dash), and equilibrium range (short dash); (e) mean (solid) and standard deviation (dashed) of $\langle S(f)\rangle$ averaged over the range f_1–f_2; (f) $I(p)$.

vides negligible improvement. The apparently strong linear relationship indicated in Fig. 8d is deceptive as inclusion of the third variate, C_p, does not add extra information to the prediction. Second, the ordinate of Fig. 8d is

$$\beta = \frac{g\langle S(f)\rangle}{8\pi I(p) u_*},$$

while the abscissa is C_p/u_*. We see that the variates of both axes are divided by u_*. Even if $\langle S(f)\rangle$, C_p, and u_* were totally uncorrelated, the figure would show an apparent correlation as this is a textbook example of a spurious correlation as described in Kenney (1982).

Accepting that β is a constant, its arithmetic mean was calculated using $u_{*\text{diss}}$ values in Eq. (3) (β = .0125

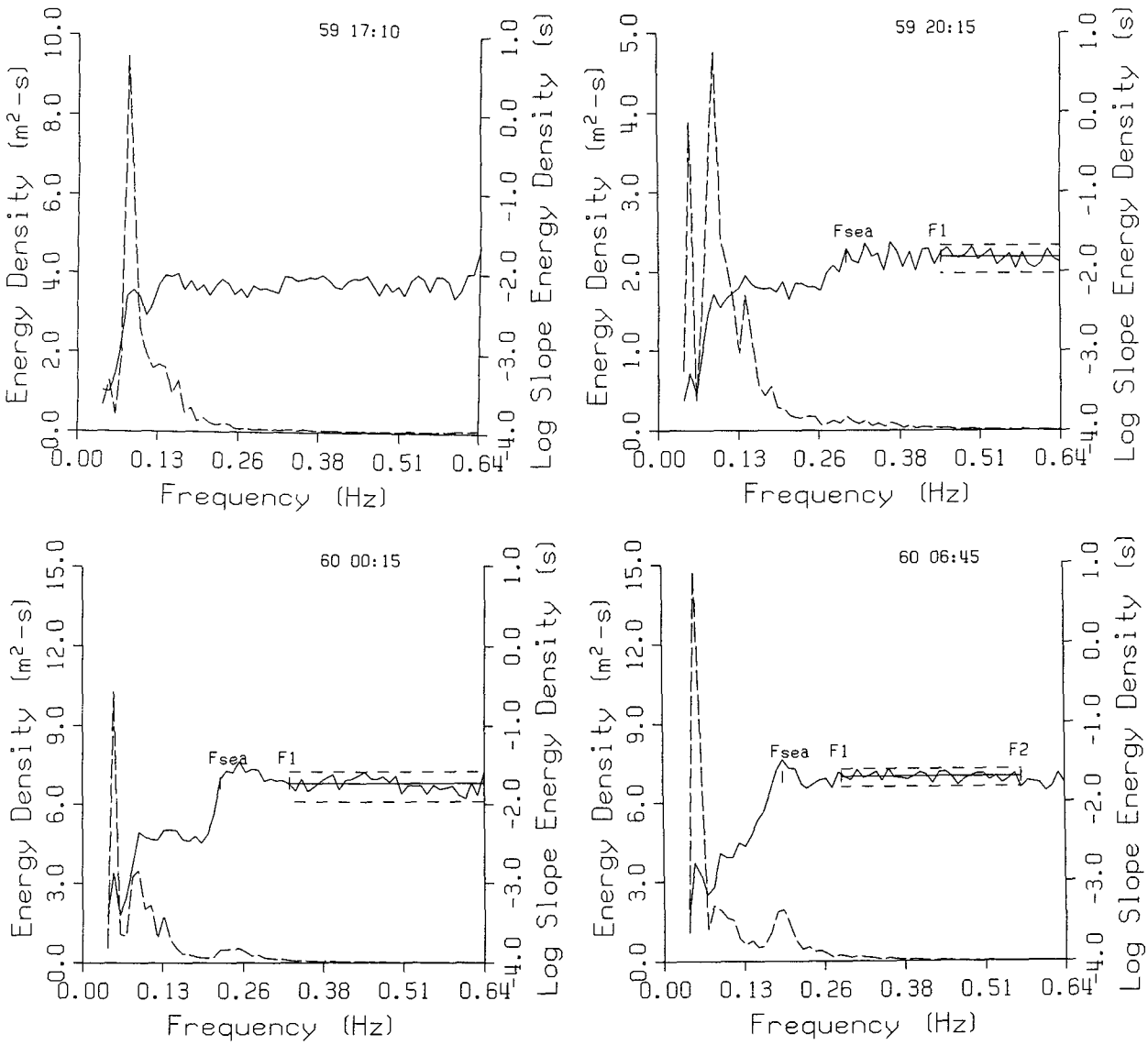

FIG. 5. Spectrum of surface displacement (dashed) and slope (solid) energy for a selected sea development period: (a) day 59 17:10; (b) 59 20:15; (c) 60 00:15; (d) 60 06:45. Also noted are the locations of f_{sea}, f_1, and f_2 ($f_2 < 0.64$); the mean slope density $\langle S(f) \rangle$ (horizontal solid line); and the standard error about the mean (horizontal dashed lines $\pm 2\sigma$).

$\pm 2.4 \times 10^{-3}$), $u_{*\text{model}}$ values ($\beta = .0122 \pm 4.0 \times 10^{-3}$), and a combined mean of $\beta = .0122 \pm 3.6 \times 10^{-3}$) was found. Regression values for β from linear prediction models were also obtained and are included in Table 1. These can be seen to be similar to the calculated means.

3) ESTIMATION OF SLOPE INFERRED u_*

Using $\beta = 0.012$ and individual record $\langle S(f) \rangle$ and $I(p)$ values measured from the slope spectra, the inferred u_* (referred to as $u_{*\text{slope}}$) were calculated and the results are shown in Fig. 9. The correlation coefficient and prediction error are given in Table 1. It can be seen in Fig. 9 that $u_{*\text{slope}}$ agree very well with both $u_{*\text{model}}$ and $u_{*\text{diss}}$ estimates and are capable of reproducing short temporal-scale variability. Here $u_{*\text{slope}}$ values always fell within the range of the 1-min $u_{*\text{diss}}$ estimates used in the 30-min averaging. The underestimate of $u_{*\text{slope}}$, or more appropriately, the overestimate of $u_{*\text{model}}$, throughout event 1 and during the buildup of event 3 are consistent with the discussion of section 3a. This behavior is also consistent with findings by other authors using dissipation u_* estimates (e.g., Smith et al. 1992; Marsden et al. 1992), which demonstrate that wave age (or surface roughness) will influence u_*. Figure 9 implies that wave age effects on u_* are more pronounced during sea buildup as there

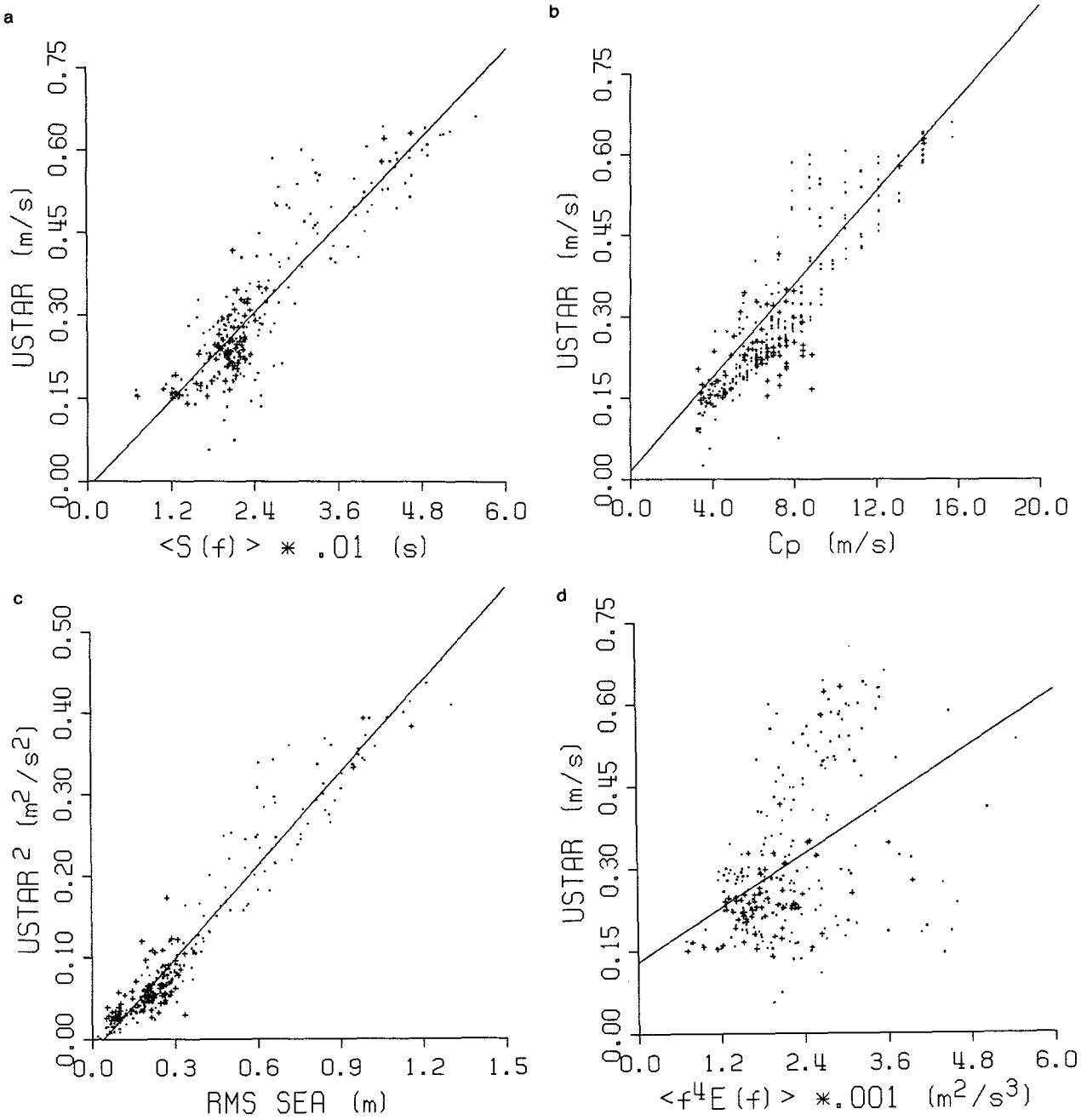

FIG. 6. Scatterplot of $u_{*\text{diss}}$ (crosses) and $u_{*\text{model}}$ (dots) measurements versus (a) $\langle S(f)\rangle$ (range from 0.0 to 0.06 s), (b) C_p, (c) rms sea wave height, and (d) $\langle f^4E(f)\rangle$ (range from 0.0 to 0.006 m^2 s^3). The linear regression of $u_{*\text{diss}}$ and the respective x-axis variable (regression coefficients listed in Table 1) are also shown on the plots.

is almost an instantaneous response of the seas during relaxation (compare the buildup and relaxation of events 1 and 3). Observations of directional spectra during relaxation also show rapid loss of high frequency (equilibrium range) energy although a "remnant" sea peak (now strictly defined as swell) can persist for some time. The absence of a lag during the buildup of event 5 and the agreement between all u_* estimates, reflects an initial surface roughness condition greater then was available prior to events 1 and 3. If one accepts that the $u_{*\text{slope}}$ estimates reflect all air–sea interaction effects on wind stress, Fig. 9 shows that Smith's boundary-layer model will, in the mean, provide good u_* values.

As seen in Table 1, the noise levels introduced by $I(p)$ resulted in an increase in prediction rms error compared with the linear regression of $\langle S(f)\rangle$ against

TABLE 1. Correlation and prediction relations between u_* and wave spectral properties.
r: correlation coefficient, $u_{*\text{diss}}$: dissipation u_* values, $u_{*\text{all}}$: $u_{*\text{diss}}$ and $u_{*\text{model}}$ values, $\langle S(f)\rangle$: mean slope spectral density, $\langle f^4 E(f)\rangle$: weighted mean amplitude spectral density, C_p: sea peak phase velocity, σ: rms sea height, $I(P)$ as defined in text, a and b are the regression parameters for the linear model $y = a + bx$ with standard error σ_a and σ_b, %rms is the percent rms error of the prediction model, and NPT is the number of points used in the analysis. Also provided are the linear prediction β values for the Phillips model (i.e., $a = 0.0$) and for a constant $\beta = 0.012$.

y	x	r	a	σ_a	b	σ_b	% rms	NPT
$u_{*\text{diss}}$	$\langle S(f)\rangle$	0.89	-3.85×10^{-2}	1.84×10^{-2}	14.02	0.875	20.4	68
$u_{*\text{all}}$	$\langle S(f)\rangle$	0.89	-1.21×10^{-2}	1.03×10^{-2}	13.25	0.405	21.3	291
$u_{*\text{diss}}$	$\langle f^4 E(f)\rangle$	0.50	9.16×10^{-2}	3.43×10^{-2}	82.15	17.57	74.5	66
$u_{*\text{all}}$	$\langle f^4 E(f)\rangle$	0.47	0.13	2.11×10^{-2}	82.09	9.32	78.1	278
$u_{*\text{diss}}$	C_p	0.79	1.63×10^{-2}	2.15×10^{-2}	3.49×10^{-2}	3.21×10^{-3}	38.0	74
$u_{*\text{all}}$	C_p	0.89	-3.01×10^{-2}	1.0×10^{-2}	4.54×10^{-2}	1.34×10^{-3}	21.1	310
$u^2_{*\text{diss}}$	σ	0.92	-9.48×10^{-3}	4.9×10^{-3}	0.34	1.7×10^{-2}	15.2	74
$u^2_{*\text{all}}$	σ	0.97	-1.56×10^{-2}	2.4×10^{-3}	3.38	5.8×10^{-3}	6.7	310
$\frac{\langle S(f)\rangle g}{8\pi I(p)}$	$u_{*\text{diss}}$	0.87	—	—	1.21×10^{-2}	0.8×10^{-3}	26.7	68
$\frac{\langle S(f)\rangle g}{8\pi I(p)}$	$u_{*\text{all}}$	0.89	—	—	1.14×10^{-2}	0.3×10^{-3}	23.8	291
$u_{*\text{diss}}$	$\frac{\langle S(f)\rangle g}{8\pi I(p)}$	0.87	—	—	1.25×10^{-2}	0.8×10^{-3}	26.5	68
$u_{*\text{all}}$	$\frac{\langle S(f)\rangle g}{8\pi I(p)}$	0.89	—	—	1.19×10^{-2}	0.3×10^{-3}	22.2	291
$u_{*\text{diss}}$	$\frac{\langle S(f)\rangle g}{8\pi I(p)}$	0.87	—	—	1.2×10^{-2}	—	27.1	68
$u_{*\text{all}}$	$\frac{\langle S(f)\rangle g}{8\pi I(p)}$	0.89	—	—	1.2×10^{-2}	—	21.9	291

u_* alone, although the regression coefficient value of 14.02 implies a requirement for a multiplicative factor of approximately 2.3, which is within the range of $I(p)$ estimates obtained. As mentioned in section 3a, there is an apparent increase in $I(p)$ during the sea growth periods; however, systematic examination with wind speed, friction velocity, or wave age did not yield conclusive results due to the high noise levels. Further field study is required to properly assess the role of $I(p)$ in the Phillips model.

Various derived quantities can be calculated from $u_{*\text{slope}}$ and compared with experimental and/or theoretical values to ascertain the reliability of the analysis procedure and to see if these u_* values truly reflect the wind

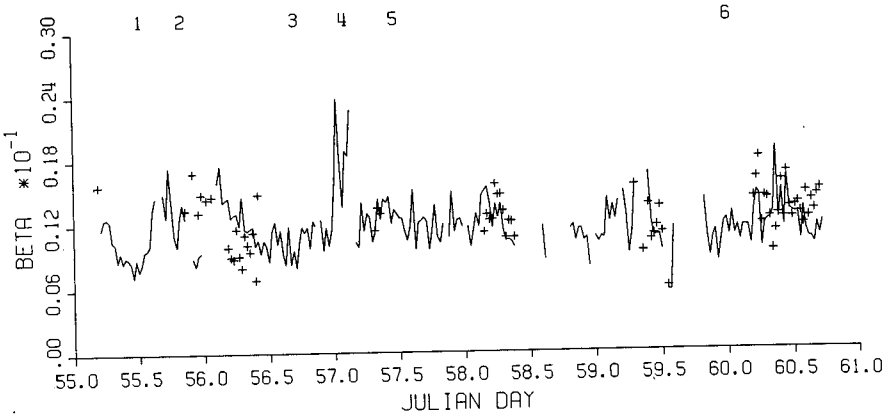

FIG. 7. Time series of β (range from 0.0 to 0.03) calculated from the $u_{*\text{model}}$ (solid) and $u_{*\text{diss}}$ (crosses) measurements.

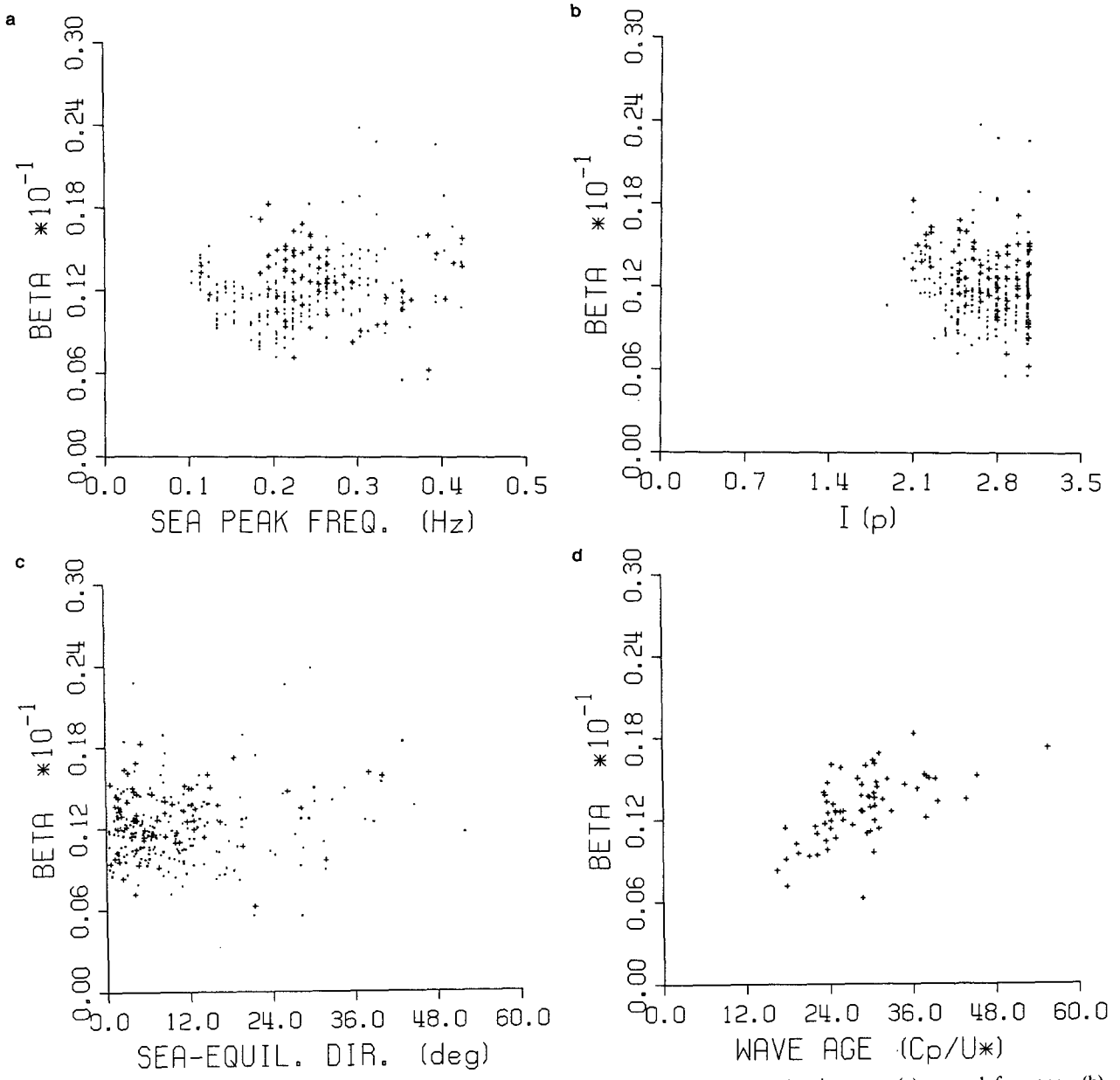

FIG. 8. Scatterplot of β (range from 0.0 to 0.03), calculated using $u_{*\text{model}}$ (dots) and $u_{*\text{diss}}$ (crosses) estimates vs (a) sea peak frequency, (b) $I(p)$, (c) difference between the sea and equilibrium range mean wave direction, and (d) wave age given as C_p/u_*.

stress operating on the waves. Toba's "constant" α_T (Toba 1973) is given as $4\beta I(p)$ (i.e., α_T would be variable in this context). The inferred α_T values lie between 0.09 and 0.15, which compare well with mean values reported in the literature, extending from 0.06 reported by Kawai et al. (1977) to 0.13 seen by Batjes et al. (1987). The roughness length z_0 or the drag coefficient C_d, defined as u_*^2/u_{10}^2, can be used to obtain u_* from u_{10} (or vice versa). These two variables were calculated with both $u_{*\text{slope}}$ and $u_{*\text{diss}}$ and the respective correlation coefficients examined. Given the high correlation between $\langle S(f) \rangle$ and $u_{*\text{diss}}$, one would also expect a significant correlation between their respective z_0 and C_d. The results show correlation coefficients of 0.72 (rms error of 49%) between z_0 values and 0.64 (rms error of 59%) for the drag coefficients with the higher errors indicating that these are inherently noisier quantities than u_*.

4. Wind stress and sea state

a. Theoretical development

As indicated by the high correlations in Table 1, wind stress (or friction velocity) is closely linked with the existing sea state. Several accepted, well-known

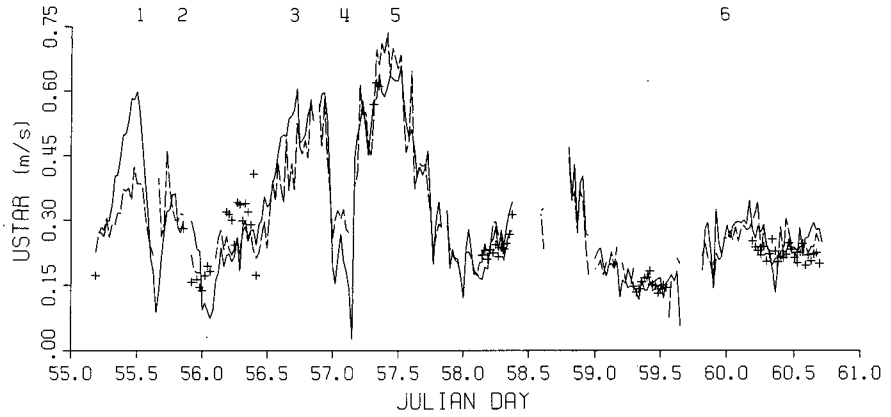

FIG. 9. Time series of $u_{*\text{model}}$ (solid), $u_{*\text{diss}}$ (crosses), and $u_{*\text{slope}}$ (dashed).

expressions can be combined with our results to provide insight into these relationships. First, Kitaigorodskii (1968) proposed the expression,

$$\frac{z_{0K}}{\sigma} = A \exp\left(-\frac{\kappa C_p}{u_*}\right) = A \exp -\left(\frac{\kappa}{C_d^{1/2}} \frac{C_p}{u_{10}}\right), \quad (10)$$

relating roughness length (z_{0K}, with the subscript K indicating Kitaigorodskii's) and rms wave height (σ) to wave age. Second, Charnock (1955) "argued on dimensional grounds that for *well-developed* seas, the roughness should be proportional to the wind stress τ" (Donelan et al. 1993):

$$z_{0C} = \frac{\alpha u_*^2}{g}. \quad (11)$$

The subscript C representing Charnock's z_{0C}. We will interpret *well-developed* seas to mean that the two roughness lengths must agree for a wave age of $C_p/u_{10} = 1.0$. And third, our empirical relationship shown in Fig. 6c and Table 1 indicates

$$u_*^2 = \gamma\sigma, \quad (12)$$

where $\gamma = 0.34$ with a compelling correlation in linear space of 0.92. That is, Eq. (12) can directly account for $(0.92)^2 = 84.6\%$ of the variability in u_*^2. Substituting Eq. (12) into Eq. (10) for σ gives

$$z_{0K} = \left(\frac{u_*^2}{\gamma}\right) A \exp\left(-\frac{\kappa}{C_d^{1/2}} \frac{C_p}{u_{10}}\right). \quad (13)$$

For Eqs. (11) and (13) to be consistent at equilibrium conditions, in the limit of $C_p/u_{10} = 1.0$, z_{0C} must equal z_{0K}. Invoking this condition and equating Eqs. (11) and (13) gives

$$\frac{\alpha u_*^2}{g} = \frac{u_*^2}{\gamma} A \exp\left(-\frac{\kappa}{C_d^{1/2}}\right) \quad (14)$$

or

$$A = \frac{\gamma\alpha}{g} \exp\left(\frac{\kappa}{C_d^{1/2}}\right). \quad (15)$$

b. Data verification

When verifying the suitability of Eqs. (10) and (15) to describe field data, the slope of the regression between $\ln(z_0/\sigma)$ and wave age (C_p/u_*) should be $-\kappa$. Since A is a function of C_d and direct verification would require the specification of the wind speed and wave age dependent C_d at every point, we need to choose a typical C_d to perform a first-order examination. The two sides of Eq. (10) are shown in Fig. 10 (a: using $u_{*\text{diss}}$ and hence values weighted by wind measurements; b: using $u_{*\text{slope}}$ giving values weighted by wave estimates). As in Fig. 8d (β versus wave age), self-correlation could be providing a "false" relationship (i.e., u_* is present in the calculation of both z_0 and wave age, see Perrie and Toulany 1990), but because it is a standard presentation in the literature (see Donelan 1990; Smith et al. 1992), we include it here. Shown on Fig. 10b is Eq. (10) with $A = 0.3$ (lower solid line) as suggested by Kitaigorodskii (1970) and the three regression relations (dashed lines) listed in Donelan (1990) for fetch-limited field and laboratory data. For verification of Eqs. (10) and (15), we let $\gamma = 0.34$ and have assumed a typical value of $C_d = 1.28 \times 10^{-3}$ (Marsden et al. 1993) based on their calculations of a constant drag coefficient independent of wind speed and wave age for moderate wind conditions. This results in an *approximate* A of 29 to 35 for $\alpha = 0.012$ to 0.014. We chose a value of $A = 30$ and plotted Eq. (10), seen as the solid line in Fig. 10a and the upper solid line in Fig. 10b. Clearly, the use of Eqs. (10) and (15) provided good agreement with the majority of the data, and it should be noted that the slope of the relation (i.e., $-\kappa$) follows the data distribution very well. This is not true for the original Kitaigorodskii expres-

sion, which, forced to have the same slope, is offset by two orders of magnitude, nor for the regression relations listed in Donelan, which, though passing through our data at young wave ages, do not have the correct functional form for our older, open ocean, fetch-unlimited measurements. The maximum observed z_0/σ value approaches the approximately 1/30 limiting ratio of roughness length to mean height of roughness elements in both Figs. 10a and 10b (See Donelan 1990.) This indicates that the slope spectra, although truncated at 0.64 Hz, can be used to resolve a full range of u_* values in the open ocean. Figures 10a,b indicate that using either set of u_* estimates to determine z_0, the observed z_0/σ behavior is similar. The cluster of lower z_0/σ values in Fig. 10b may be due to experimental noise, an error in the estimate of one of the variates or these values may be real. The individual estimates of C_p were verified visually and found to be correct. Given the observed range in the sea rms wave heights and their low noise behavior in Fig. 6c, they could not be the cause of a vertical error (z_0/σ) of as much as four orders of magnitude. A possible experimental source of error could arise when performing the wind speed height adjustment to 10 m, using Eq. (5) without including a wave age dependence on z_0. However, this is expected to be minor if the wave age correction is only of "second order." The data values may be real and the variable nature of A [Eq. (15)] would not only allow for adjustment of Eq. (10) to pass through these points, it may also reconcile these results with those from fetch-limited studies.

c. *Drag coefficient as a function of wind speed and wave age*

A general solution for the functional relationship between C_d and wind speed (or friction velocity) and wave age can be achieved by incorporating the law of the wall (Eq. 5) into our analysis. Substituting Eq. (15) into Eq. (13) and dropping the subscript K gives

$$z_0 = \frac{u_*^2 \alpha}{g} \exp\left(\frac{\kappa}{C_d^{1/2}} - \frac{\kappa C_p}{u_*}\right). \tag{16}$$

From Eq. (5) we get

$$z_0 = z \exp\left(-\frac{\kappa}{C_d^{1/2}}\right). \tag{17}$$

Substituting Eq. (17) into Eq. (16) gives

$$\frac{zg}{\alpha} = u_*^2 \exp\left(\frac{2\kappa}{C_d^{1/2}} - \frac{\kappa C_p}{u_*}\right) \tag{18a}$$

in terms of u_* and

$$\frac{zg}{\alpha} = C_d u_{10}^2 \exp\left[\frac{\kappa}{C_d^{1/2}}\left(2 - \frac{C_p}{u_{10}}\right)\right] \tag{18b}$$

in terms of u_{10}. Given a standard measurement height of 10 m, one can solve Eq. (18a) directly for C_d as a function of u_* and wave age (C_p/u_*) and Eq. (18b) iteratively for C_d as a function of wind speed and wave age (C_p/u_{10}). The results are shown in Figs. 11a,b. The predicted drag coefficients show behavior consistent with expectations: C_d increases with u_* (or u_{10}) at a

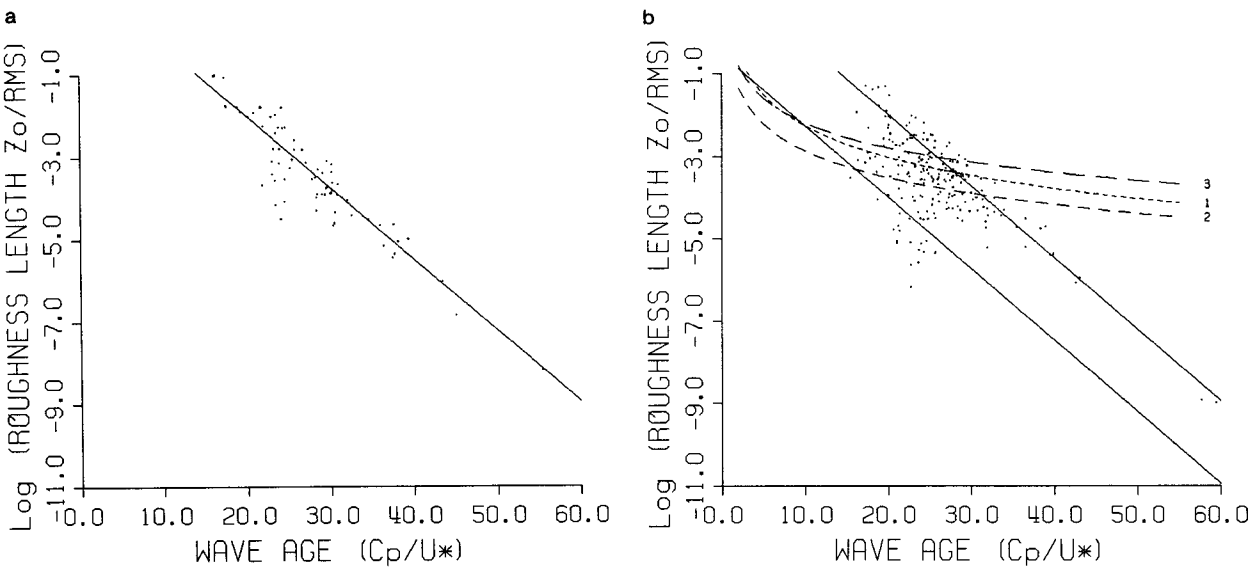

FIG. 10. Relationship of nondimensional roughness (z_0/σ), using (a) $u_{*\text{diss}}$ and (b) $u_{*\text{slope}}$, as a function of wave age. The solid line in 10a and upper solid line in 10b is an Eq. (10) with $A = 30$. The numbered dashed lines correspond to the regression $z_0/\sigma = A(u_*/C_p)^B$ from Donelan (1990, Table II), where 1) $A = 1.84$, $B = 2.53$; 2) $A = 0.205$, $B = 2.18$; and 3) $A = 0.637$, $B = 2$. The lower solid line in (b) is a plot of Eq. (10) with Kitaigorodskii's choice of $A = 0.3$.

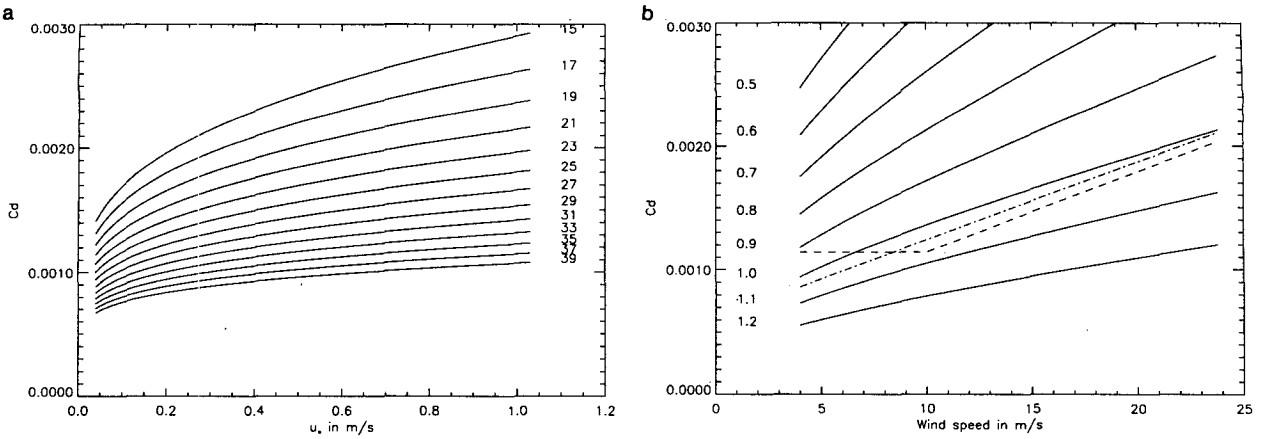

FIG. 11. Predicted drag coefficients as a function of (a) u_* and wave age (C_p/u_*) and (b) wind speed and wave age (C_p/u_{10}). The inset numbers indicate the wave age. The dot–dashed line in Fig. 11b is the C_d vs wind speed relationship of Smith (1980) and the dashed line is that of Large and Pond (1981).

given wave age and decreases with wave age for a given u_* (or u_{10}). For comparison, we include the directly measured wind speed dependences of C_d from Large and Pond (1981) and Smith (1980). A wave age (C_p/u_{10}) of 1 indicates an equilibrium sea and of 1.2 a fully mature sea. Clearly, the theoretical extension of our results is in close agreement with directly measured C_d in both amplitude and slope for equilibrium conditions using completely independent data. Since wave age effects are expected to be strongest at low wind speeds (i.e., veering, rising and falling winds), the Large and Pond (1981) constant drag coefficient in the low wind speed regime may reflect an average of drag coefficients over this sensitive wind regime. It should be noted that the isopleths shown in Fig. 11b are the theoretical values derived from Eq. (18b) and not all combinations of wind speed–wave age may be attainable or measurable. In particular, the 30-minute averaging required in the wave spectral analysis could obscure the air–sea relationships during the very rapid early spectral growth expected under high wind conditions.

Ultimately, the purpose of the wave age correction is to increase the predictability of u_* from u_{10} (or vice versa) through the drag coefficient (C_{d10}). An estimate of the prediction of C_{d10} from u_* alone can be found by equating the Charnock relation [Eq. (11)] to the law of the wall [Eq. (17)] to get

$$\frac{\alpha u_*^2}{g} = z \exp\left(\frac{-\kappa}{C_d^{1/2}}\right), \tag{19}$$

while Eq. (18a) can be inverted to give an estimate of C_d that also includes wave age C_p/u_*. Figure 12a shows the directly measured (i.e., using anemometer u_{10} and $u_{*\mathrm{diss}}$) and predicted drag coefficients with no wave age correction using Eq. (19). The solid line represents equality. The results are clearly scattered with a correlation coefficient of only 0.36, indicating that only 13% of the data variance is being accounted for. The equality line passes through the center of mass of the scatter, which is expected given that wave age effects would represent a perturbation about the Charnock relationship, which holds for equilibrium seas. Figure 12b shows the directly measured versus predicted drag coefficients with the u_* and wave age dependence based on Eq. (18a). The correlation coefficient has increased to 0.88, suggesting that 77% of the variance is now being accounted for and the scatter follows the line of equality much more closely. There still exists some disagreement between the data and the theory, but clearly there has been a marked improvement in predictability. These results not only prove that the theoretical development leading to Eq. (18a) was not incestuous, they also suggest that the wave age correction may be greater than the second-order correction generally assumed. As the data drag coefficients were calculated from 10-m winds, initially measured at 19.5 m and corrected to this standard height through z_0, the lack of wave age dependence in z_0 may account for the remaining unexplained variance. Smith et al. (1992) also supply a formulation to predict C_d from u_* and wave age based on observations during HEXOS in the North Sea. Their predicted drag coefficients, using our input wind and wave measurements, were treated in a similar manner, and it was found that the correlation coefficient was 0.55 (i.e., explaining 30% of the variance), suggesting that their wave age correction was insufficient for our open ocean data.

In summary, by assuming that the Kitaigorodskii (1968) form of wave age dependence with roughness length must agree with the Charnock (1955) form in the equilibrium limit and incorporating our strong empirical relationship between σ and u_*^2, we arrive at a closed form relationship for the multiplier A, which is found to be a function of the drag coefficient C_d. We assumed initially a constant drag coefficient and demonstrated good agreement between the variates of Eq.

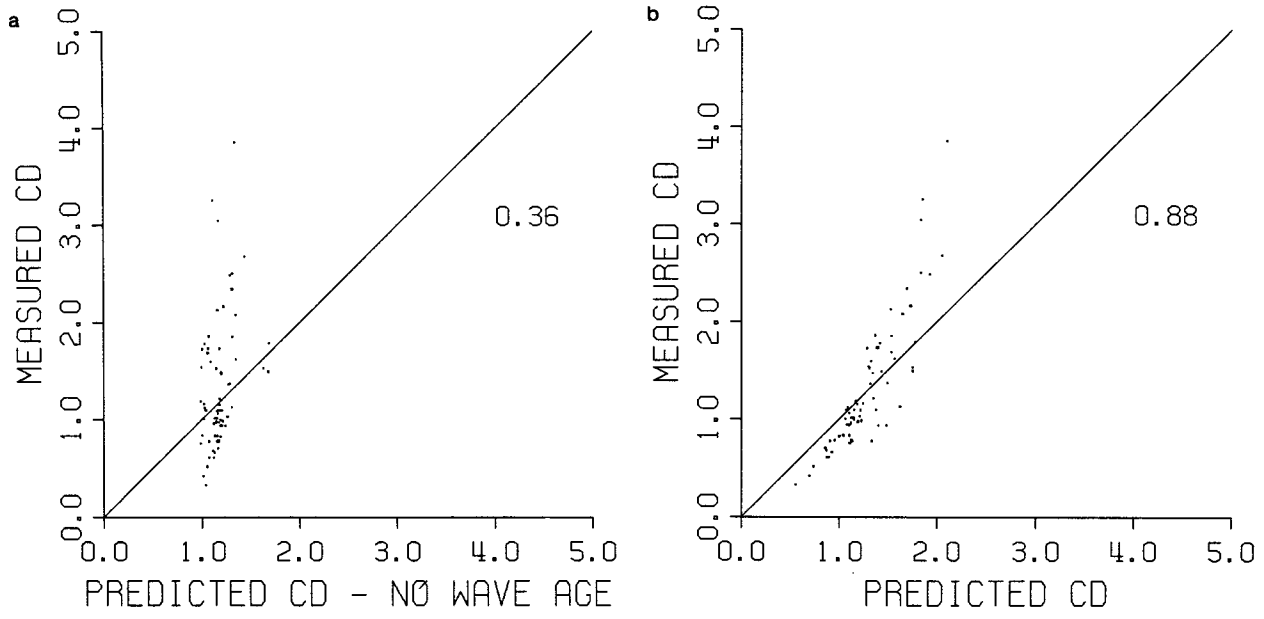

FIG. 12. Directly measured vs predicted C_d obtained by (a) inversion of the Charnock relation (i.e., no wave age dependence) and (b) inversion of Eq. (18a) (i.e., u_* wave age dependence included). The solid line represents equality and the correlation coefficient is noted beside it.

(10) over the complete range of directly measured roughness lengths and wave ages (Fig. 10a). The scatter about the curves can be explained through not including the second-order wave age and wind speed dependence in A through C_d. Furthermore, through inclusion of the law of the wall in the analysis to solve for z_0, we arrive at a relationship between C_d and wind speed or friction velocity in isopleths of wave age. The predicted relationship agrees almost identically with the directly measured, open ocean results of Large and Pond (1981) and Smith (1980) for equilibrium seas. The agreement between the experimental and predicted drag coefficient, with and without the wave age dependence, showed marked improvement when our wave age dependence relationship was included, thereby acting as an independent verification of Eq. (18a).

5. Summary and discussion

We have shown that wave field properties are highly correlated with the wind friction velocity, that the measured slope spectra are consistent with the Phillips model and allow for an estimate of the universal constant β, and that $u_{*\text{slope}}$ values agree well with both dissipation and boundary-layer model stresses. In the latter case, discrepancies can be directly attributed to wave age corrections absent in the model. Analysis of the influence of wave age on derived roughness lengths exhibited similar behavior for both the slope and dissipation estimates, allowed for an examination of the consistency between various air–sea interaction relationships and the establishment of a general expression for the drag coefficient as a function of friction velocity, wind speed, and wave age. Our findings, therefore, appear to validate the Phillips (1985) model of the wavenumber spectrum for the equilibrium range of wind-driven seas and indicate that Smith's (1988) boundary-layer model provides good first-order stress estimates.

There are certain features of this experiment worth noting. First, both the experimental design and location provided excellent air–sea environmental measurements to allow an understanding of fetch-unlimited, deep water response for which most of the theory is derived. Second, it showed that an analysis of directional wave information in wavenumber space was not required if care were taken in removing contamination due to potential Doppler shift effects. Hence, a single surface-following buoy can provide as much information as either an array of moored sensors or remote wavenumber spectral measurement methods. Third, the flat nature of the slope spectrum in the equilibrium range, accepting deep-water dispersion relationships, can only occur with a ω^{-4} dependence of the amplitude spectrum. Fourth, long-period swell, present throughout the experiment, did not appear to contribute significantly to either the rms sea calculation or the $u_{*\text{slope}}$ values. At our 30-minute temporal resolution, no time lag was observed between the wave energy response (both amplitude and slope) and wind stress. Fifth, the experiment showed that very high correlations exist between wave spectral properties and wind friction velocity possibly allowing for operational applications. The directly measured slope signal provided a better estimate of u_* than an equivalent signal obtained by

multiplying the amplitude spectrum by ω^4. Sixth, even given the presence of experimental noise and a source of uncertainty in the calculation of $I(p)$, a full range in u_* and z_0 could be resolved from the wave slope information. And seventh, we showed that by assuming that the Kitaigorodskii (1968) form of wave age dependence with roughness length must agree with the Charnock (1955) form in the equilibrium limit, and then incorporating our strong empirical relationship between rms height and friction velocity, could lead to an air–sea interaction relationship consistent with the data and in which the effects of wind speed dependence and wave age enter through a variable drag coefficient. We then provided a generalized expression for the calculation of C_d, in terms of wind speed or friction velocity and wave age, which agreed well with independent data and was verified by comparing directly measured against predicted drag coefficients, with and without the wave age dependence included. The primary limitations of the study were the lack of dissipation measurements during the higher energy wind events possibly biasing some of the results and the high level of noise in the $I(p)$ estimates, which limits our understanding on the role it plays in the Phillips model.

Some confusion appears to exist in the literature concerning both the universal nature and value of the momentum transfer constant (β or α, symbols used interchangeably by various authors) and about the actual shape of the wavenumber (or frequency) spectrum. Accepting Phillips theory β, from the wavenumber representation, should be the universal constant with a value indicated by the slope spectra of approximately 0.012. Its universality was tested against a large wave age range (from 12 to 60), although limited to low wind speeds, and no statistically significant relationship existed. Since our study may be biased to a low wind regime, this premise should be tested further under high-energy conditions. In fetch-limited locations, the influence of the advective term in Eq. (1) would have to be assessed. Confusion regarding the shape of the spectrum may be linked to the range of wavenumbers (or frequencies) being examined by various authors. For example, Banner et al. (1989), examining the equilibrium range for wavelengths between 0.2 and 1.6 m (note, our study wavelengths are greater than 3.7 m), indicate a spectral shape inconsistent with the Phillips model. These authors also note, however, that within their wavenumber range, they did not see a dependence on u_* as observed at both higher and lower wavenumbers and go on to suggest that the Phillips model may apply at the lower wavenumbers. This observed lack of wind response may correspond to the "spectral gap" proposed by Phillips (1985). Numerous other theoretical and statistical results were proposed by Phillips, and their verification against field measurements will be the focus of future work.

Acknowledgments. We appreciate immensely the meticulous air–sea synoptic atmospheric observations provided to us by Jeff Hanson and Larry White of The Johns Hopkins University. We appreciate (not to mention were amazed) that Dr. Fred Dobson of the Bedford Institute of Oceanography allowed us to let his WAVEC drift freely in the North Pacific Ocean. We also thank Dr. David Farmer of the Institute of Ocean Sciences for asking us to participate in the project and for providing administrative support. Randy Kashino of Axys Marine Consulting was our shipboard representative, and his technical skill in collecting the data was crucial to the success of the project. We thank Dr. Stuart Smith of the Bedford Institute of Oceanography for his comments and encouragement during the initial writing of the paper and an unknown reviewer whose questions led to a more rigorous analysis of the data and the development of the air–sea relationships of section 4. RFM and SRW were supported by Allocations 3705-833 (FUHHH) and 3705-876 (FUHHI), respectively, of the Academic Research Program of the Department of National Defense of Canada.

REFERENCES

Banner, M. L., 1991: On the directional behavior of the equilibrium wave number spectrum: Implications for the equilibrium frequency spectrum. *Directional Ocean Wave Spectra,* R. C. Beal, Ed., The Johns Hopkins University Press, 39–45.

——, I. S. F. Jones, and J. C. Trinder, 1989: Wavenumber spectra of short gravity waves. *J. Fluid Mech.,* **198,** 321–344.

Battjes, J. A., T. J. Zitman, and L. H. Houlthiujsen, 1987: Reanalysis of the spectra observed in JONSWAP. *J. Phys. Oceanogr.,* **17,** 1288–1295.

Charnock, H., 1955: Wind stress on a water surface. *Quart. J. Roy. Meteor. Soc.,* **81,** 639–640.

Cox, C., and W. Munk, 1954: Statistics of the sea surface derived from sun glitter. *J. Mar. Res.,* **13,** 198–227.

Dobson, F., W. Perrie, and B. Toulany, 1989: On the deep-water fetch laws for wind-generated surface gravity waves. *Atmos.-Ocean,* **27,** 210–236.

Donelan, M. A., 1990: Air–sea interaction. *The Sea,* Vol. 9A, Wiley Interscience, B. Le Mehaute and D. M. Hanes, Eds., 239–292.

——, J. Hamilton, and W. H. Hui, 1985: Directional spectra of wind-generated waves. *Philos. Trans. Roy. Soc. London/Ser. A,* **315,** 509–562.

——, F. Dobson, S. D. Smith, and R. A. Anderson, 1993: On the dependence of sea surface roughness on wave development. *J. Phys. Oceanogr.,* **23,** 2143–2149.

Kawai, S., K. Okuda, and Y. Toba, 1977: Field data support of three-seconds power law and $gu_*\omega$-4 spectral form for growing wind waves. *J. Oceanogr. Soc. Japan,* **33,** 137–150.

Kenney, B. C., 1982: Beware of spurious self-correlations! *Water Resour. Res.,* **18,** 1041–1048.

Kitaigorodskii, S. A., 1968: On the calculation of the aerodynamic roughness of the sea surface. *Bull. Acad. Sci. USSR, Atmos. Oceanic Phys.,* **4,** 870–878.

——, 1970: *The Physics of Air–Sea Interaction.* Israel Program for Scientific Translations, 1973, 237 pp.

Large, W. G., and S. Pond, 1981: Open ocean momentum flux measurements in moderate to strong winds. *J. Phys. Oceanogr.,* **11,** 324–336.

Marsden, R. F., 1987: A comparison between geostrophic and directly measured surface winds over the Northeast Pacific Ocean. *Atmos. Ocean,* **25,** 387–401.

——, and B.-A. Juszko, 1987: An eigenvector method for the calculation of directional spectra from heave, pitch and roll buoy data. *J. Phys. Oceanogr.,* **17,** 2157–2167.

——, and ——, 1989: Wind estimates from wave slopes. *J. Geophys. Res.*, **94,** 6266–6272.

——, G. A. McBean, and B. A. Proctor, 1993: Momentum and sensible heat fluxes calculated by the dissipation technique during the Ocean Storms project. *Bound.-Layer Meteor.*, **63,** 23–38.

Perrie, W., and B. Toulany, 1990: Fetch relations for wind-generated waves as a function of wind-stress scaling. *J. Phys. Oceanogr.*, **20,** 1666–1681.

Phillips, O. M., 1985: Spectral and statistical properties of the equilibrium range in wind-generated gravity waves. *J. Fluid Mech.*, **156,** 505–531.

Smith, S. D., 1980: Wind stress and heat flux over the ocean in gale force winds. *J. Phys. Oceanogr.*, **10,** 709–726.

——, 1988: Coefficients for sea surface wind stress, heat flux, and wind profiles as a function of wind speed and temperature. *J. Geophys. Res.*, **93,** 15 467–15 472.

——, R. J. Anderson, W. A. Oost, C. Kraan, N. Maat, J. DeCosmo, K. B. Katsaros, K. L. Davidson, K. Bumke, L. Hasse, and H. M. Chadwick, 1992: Sea surface wind stress and drag coefficients: the HEXOS results. *Bound.-Layer Meteor.*, **60,** 109–142.

Toba, Y., 1973: Local balance in the air–sea boundary processes. III. On the spectrum of wind waves. *J. Oceanogr. Soc. Japan,* **29,** 209–220.